Convergent molecular, cellular, and cortical neuroimaging signatures of major depressive disorder

Kevin M. Anderson[a,1], Meghan A. Collins[a], Ru Kong[b,c,d,e,f], Kacey Fang[a], Jingwei Li[b,c,d,e,f], Tong He[b,c,d,e,f], Adam M. Chekroud[g,h], B. T. Thomas Yeo[b,c,d,e,f,i], and Avram J. Holmes[a,g,j]

[a]Department of Psychology, Yale University, New Haven, CT 06520; [b]Department of Electrical and Computer Engineering, National University of Singapore, Singapore; [c]Centre for Sleep and Cognition, National University of Singapore, Singapore; [d]Clinical Imaging Research Centre, National University of Singapore, Singapore; [e]N.1 Institute for Health, National University of Singapore, Singapore; [f]Institute for Digital Medicine, National University of Singapore, Singapore; [g]Department of Psychiatry, Yale University, New Haven, CT 06520; [h]Spring Health, New York, NY 10001; [i]Graduate School for Integrative Sciences and Engineering, National University of Singapore, Singapore; and [j]Department of Psychiatry, Massachusetts General Hospital, Harvard Medical School, Boston, MA 02114

Edited by Huda Akil, University of Michigan, Ann Arbor, MI, and approved August 12, 2020 (received for review May 5, 2020)

Major depressive disorder emerges from the complex interactions of biological systems that span genes and molecules through cells, networks, and behavior. Establishing how neurobiological processes coalesce to contribute to depression requires a multiscale approach, encompassing measures of brain structure and function as well as genetic and cell-specific transcriptional data. Here, we examine anatomical (cortical thickness) and functional (functional variability, global brain connectivity) correlates of depression and negative affect across three population-imaging datasets: UK Biobank, Brain Genomics Superstruct Project, and Enhancing NeuroImaging through Meta Analysis (ENIGMA; combined $n \geq 23{,}723$). Integrative analyses incorporate measures of cortical gene expression, postmortem patient transcriptional data, depression genome-wide association study (GWAS), and single-cell gene transcription. Neuroimaging correlates of depression and negative affect were consistent across three independent datasets. Linking ex vivo gene down-regulation with in vivo neuroimaging, we find that transcriptional correlates of depression imaging phenotypes track gene down-regulation in postmortem cortical samples of patients with depression. Integrated analysis of single-cell and Allen Human Brain Atlas expression data reveal somatostatin interneurons and astrocytes to be consistent cell associates of depression, through both in vivo imaging and ex vivo cortical gene dysregulation. Providing converging evidence for these observations, GWAS-derived polygenic risk for depression was enriched for genes expressed in interneurons, but not glia. Underscoring the translational potential of multiscale approaches, the transcriptional correlates of depression-linked brain function and structure were enriched for disorder-relevant molecular pathways. These findings bridge levels to connect specific genes, cell classes, and biological pathways to in vivo imaging correlates of depression.

major depressive disorder | neuroimaging | gene expression | somatostatin interneurons | astrocytes

Major depressive disorder (MDD) is a common and debilitating illness with a moderately strong genetic basis (heritability, $h^2 \approx 40\%$) (1). Clinical depression emerges through complex interactions spanning multiple biological systems and levels of analysis (2). The multiscale nature of depression is evident in the presence of disorder-relevant genetic loci (3), as well as shifts in gene expression (4, 5), cellular composition (6, 7), cortical anatomy (8), and large-scale network function (9). However, most human research on the pathophysiology of depressive illness focuses on select features of brain biology, often in isolation. For instance, in vivo neuroimaging studies link symptom profiles in patients to brain anatomy and network function (10, 11), but are largely divorced from insights about underlying molecular and cellular mechanisms. By contrast, analyses of postmortem tissue samples characterize illness-related cellular and biological processes (4, 5, 12, 13), but often focus on few regions and are limited by coarse diagnostic detail. To date, there have been few opportunities to directly explore the depressive phenotype across levels of analysis—from genes and molecules through cells, circuits, networks, and behavior—simultaneously (14).

In vivo neuroimaging has identified depression-related correlates in brain anatomy, metabolism, and function. For example, discoveries linking amygdala–medial prefrontal cortex (mPFC) circuitry to emotional (15) and social processing (16) led to the hypothesis that dysregulated interactions of cortical and subcortical systems precipitate the onset of depression (2, 17). Disrupted metabolism and altered gray matter volume in the mPFC of patients is also a pronounced feature of the disorder (8, 18) that may track illness chronicity (19). As sample sizes have increased into the thousands, however, it is apparent that many early identified effects are likely more subtle than initially expected

Significance

Major depressive disorder is a debilitating condition with diverse neuroimaging correlates, including cortical thinning in medial prefrontal cortex and altered functional connectivity of cortical association networks. However, the molecular bases of these imaging markers remain ambiguous, despite a need for treatment targets and mechanisms. Here, we advance cross-modal approaches to identify cell types and gene transcripts associated with depression-implicated cortex. Across multiple population-imaging datasets (combined $N \geq 23{,}723$) and ex vivo patient cortical tissue, somatostatin interneurons and astrocytes emerge as replicable cell-level correlates of depression and negative affect. These data identify transcripts, cell types, and molecular processes associated with neuroimaging markers of depression and offer a roadmap for integrating in vivo clinical imaging with genetic and postmortem patient transcriptional data.

Author contributions: K.M.A. and A.J.H. designed research; K.M.A. performed research; K.M.A., R.K., J.L., T.H., and B.T.T.Y. contributed new reagents/analytic tools; K.M.A. analyzed data; K.M.A., A.M.C., and A.J.H. wrote the paper; and M.A.C., R.K., K.F., J.L., T.H., A.M.C., B.T.T.Y., and A.J.H. contributed analytic expertise, theoretical guidance, paper revisions, and informed interpretation of the results.

Competing interest statement: A.M.C. holds equity in Spring Care Inc, Fitbit Inc, and UnitedHealthcare Inc. He is lead inventor on three patent submissions relating to treatment for major depressive disorder (US Patent and Trademark Office [USPTO] docket no. Y0087.70116US00, USPTO provisional application no. 62/491,660, and USPTO provisional application no. 62/629,041). He has consulted for Fortress Biotech on antidepressant drug development.

This article is a PNAS Direct Submission.

[1]To whom correspondence may be addressed. Email: kevin.anderson@yale.edu.

This article contains supporting information online at https://www.pnas.org/lookup/suppl/doi:10.1073/pnas.2008004117/-/DCSupplemental.

First published September 21, 2020.

(8, 20). As a consequence, the stability of depression-relevant profiles of brain anatomy and function across populations remains unclear.

Complex clinical phenotypes like depression are tied to interactions throughout the functional connectome (9, 10, 21). Supporting this perspective, biological subtypes and heterogeneous presentations of depression may be revealed by considering the collective set of functional connections in the brain (10, 11). Spatially diffuse correlates of depression across cortical anatomy and function could arise from a host of biological changes in patient populations, such as altered neurotransmission (22), inflammation (23), and changes in cell abundance or morphology (6). Approaches that consider cross-level neurobiological relationships would illuminate the biological bases of large-scale neuroimaging correlates of depressive illness. The emergence of whole-brain gene expression atlases (24) now permits more spatially comprehensive descriptions of the transcriptional correlates of in vivo depression phenotypes, complementing targeted ex vivo analyses of select cortical areas.

Analyses of postmortem MDD patient data have revealed abnormalities across cell classes, neurotransmitter systems, and molecular pathways (6, 7, 25). For instance, diagnosis of depression is associated with reduced cell size and abundance of neurons and glia within prefrontal cortex (18, 26) and subgenual aspects of mPFC (6, 7). In particular, dysfunction of cortical somatostatin (SST) interneurons and astrocytes are hypothesized to play a preferential role in depression onset (12, 13, 27). However, broad disruptions across molecular processes have been documented, including depression-related dysregulation of pathways related to apoptotic stress and neuroinflammation (28, 29), g-coupled protein receptors (GPCR) and cytokine activity (4), and ERK signaling and excitatory neuron activity (5), as well as extensive alterations that encompass many major neurotransmitter signaling systems (25). The breadth of observed neurochemical disruptions in depression makes parsimonious descriptions of the disorder difficult. Moreover, the degree of diagnostic specificity linking depression-relevant patterns of brain anatomy and function with any given cellular or molecular abnormality remains unclear.

In this study, we identify shared neurobiological signatures of depression that link anatomical, functional, cellular, transcriptional, and genetic levels of analysis. Using three imaging datasets (combined $n \geq 23{,}723$), we quantify cortical structural and functional correlates of depression and negative affect that are consistent across populations. Multiple biological hypotheses about the neural substrates of depression have been proposed, such as interneuron and glial cell dysfunction, as well as alterations in glutamatergic signaling (12, 13, 30). However, most neuroimaging modalities are not sensitive to underlying molecular or transcriptional properties of brain tissue. To address this gap, we link cortical correlates of depression to normative patterns of gene expression in the adult human brain, identifying cell classes and gene transcripts expressed most within depression-implicated brain regions. Indicating that normative patterns of gene expression may inform depression-related vulnerability of cortex, the transcriptional associates of depression neuroimaging phenotypes correlated with gene dysregulation in independent MDD ex vivo patient brain tissue. Postmortem case–control data also identified cell types tied to both in vivo signatures of depression and dysregulation in ex vivo brain tissue of patients. Given the retrospective nature of both the neuroimaging and postmortem patient data, enrichment analyses of genome-wide association study (GWAS) results were conducted to identify cells with increased polygenic burden linked to depression. Taken together, these data identify stable imaging correlates of depression across populations, highlighting the role of SST interneurons and astrocytes, and define a roadmap for future multiscale neuroscience research on transcriptional bases of brain structure, function, and risk for depression.

Results

Neuroimaging Correlates of Depression and Negative Affect Are Consistent across Populations. We first characterize the nature and stability of cortical imaging markers of depression and trait negative affect by analyzing structural and functional MRI data from three independent large-scale collection efforts: UK Biobank (UKB) (31), ENIGMA (8), and Brain Genomics Superstruct Project (GSP) (32). Our analyses of multiple datasets are meant to increase statistical power and reduce potential dataset-specific biases in recruitment or the manner that depression and trait negative affect were measured (33). Three imaging measures were examined: cortical thickness, resting-state functional amplitude (RSFA), and global brain connectivity (GBC). In the UKB (n = 15,150), lifetime history of depression was determined from questionnaires collected at the MRI scan visit (see *Methods*). Readers should note that RSFA is influenced by

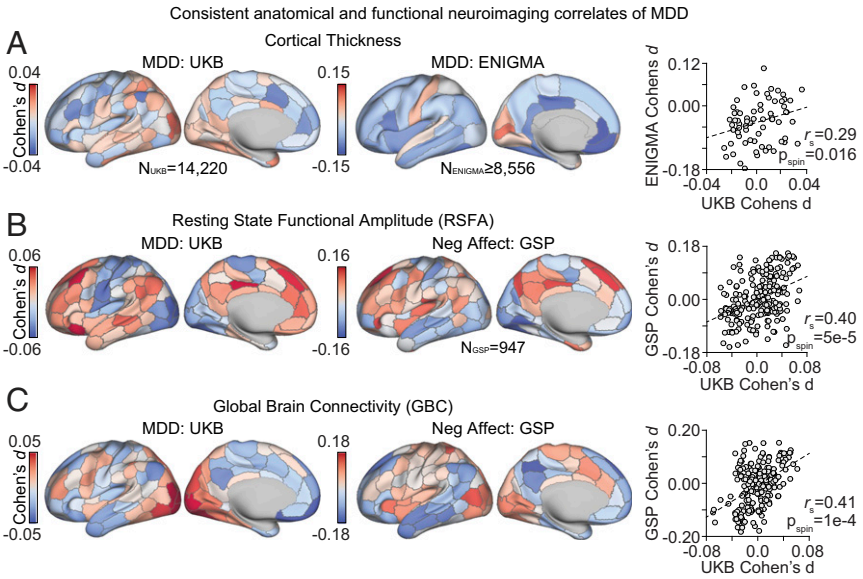

Fig. 1. Consistent imaging correlates of depression and negative affect across datasets. (*A*) Differences in cortical thickness between moderate/severe recurrent MDD and controls in the UKB and ENIGMA, and their spatial correlation ($r_s = 0.29$). Association of (*B*) RSFA and (*C*) GBC to moderate/severe MDD in the UKB, and negative affect in the GSP, and their spatial correlation (RSFA: $r_s = 0.40$; GBC: $r_s = 0.41$). Each dot represents one of 200 parcels from the functional atlas from Schaefer et al. (34). Significance was established using permuted spin tests to retain the structure of spatial autocorrelation of effects. UKB effects reflect comparison of n = 2,136 individuals with lifetime history of recurrent MDD (controls, n = 12,223). ENIGMA data are metaanalytic estimates of MDD (ns = 1,206 to 1,302) relative to controls (ns = 7,350 to 7,449) (8). GSP data reflect relationships to a continuous measure of trait negative affect in n = 947 healthy young adults. Dashed line is the regression line of best fit.

cerebrovascular factors and should not be interpreted as a direct measure of neural activity (*SI Appendix*). Further, the depression phenotype in the UKB is a retrospective measure of lifetime depressive illness and does not indicate an active depressive episode at the time of the scan. The validity of the UKB depression phenotype was explored by comparison with related self-report measures. Single (5.22%, n = 791), moderate recurrent (9.93%, n = 1,505), and severe recurrent (4.17%, n = 631) depression were significantly positively associated with trait neuroticism, depressive symptom severity, genetic risk for depression estimated through prior GWAS (3), and rate of antidepressant prescription (*SI Appendix*, Fig. S1). Replication ENIGMA (Enhancing NeuroImaging Genetics through Meta-Analysis) data reflect metaanalytic results from Schmaal et al. (8) showing shifts in cortical thickness in patients with depression (n = 1,206 to 1,302) relative to healthy comparison participants (n = 7,350 to 7,449). In the GSP sample (n = 947), trait negative affect was measured in healthy young adults using five convergent self-report questionnaires associated with the experience of negative mood (see *Methods*). Overall, the use of multiple datasets and phenotypic measures helps to identify generalizable brain correlates of depression history and risk for possible onset (trait negative affect) in healthy populations.

We identified structural and functional correlates of depression that were consistent across datasets, measures of depression, and imaging modalities. Fig. 1 displays whole-cortex results from regression analyses, conducted separately across 200 symmetric regions from the parcellation of Schaefer et al. (34). In the UKB, multiple regression revealed relationships between history of recurrent depression (0/1) and cortical thickness, RSFA, and GBC (Fig. 1), partialing out demographic and technical covariates (see *Methods* and Dataset S1 *A–F*). Including self-reported antidepressant use as a covariate had very little effect on the imaging correlates of depression: Spatial correlations (r) with and without antidepressant were >0.93. This suggests that cortical correlates of depression history are not solely driven by pharmacological effects (*SI Appendix*). Parallel analyses in the GSP dataset revealed whole-cortex relationships between trait negative affect and RSFA and GBC. ENIGMA data reflected published metaanalytic results from Schmaal et al. (8), comparing cortical thickness in MDD patients relative to controls. Effects are quantified with Cohen's d to make results comparable among datasets.

Across UKB, ENIGMA, and GSP imaging datasets, we observed spatially consistent correlates of depression and negative affect for thickness (r_s = 0.29, P = 0.018, p_{spin} = 0.016), RSFA (r_s = 0.40, P = 4.7e-9, p_{spin} = 5e-5), and GBC (r_s = 0.41, P = 2.3e-9, p_{spin} = 1e-4; r_s = Spearman's Rho; p_{spin} = spin based permutation p-value; Fig. 1). Spatial consistency was quantified as the Spearman's correlation of Cohen's d effect sizes between two imaging maps. Significance testing used spin-based permutations to account for spatial autocorrelation among parcels (35, 36). Consistent with the theorized core role for disrupted heteromodal association cortex functioning in psychiatric illness (37), depression-relevant shifts in RSFA and GBC were preferential to heteromodal relative to unimodal cortices. That is, depression-linked Cohen's d for RSFA was greater in heteromodal (M = 0.018 ± 0.025[SD]) compared to unimodal cortices (−0.026 ± 0.023; p_{perm} = 0.001; $p_{perm=permutation\ based\ p\text{-}value}$). By contrast, GBC effects were lower in heteromodal (−0.003 ± 0.021) relative to unimodal cortex (0.008 ± 0.03, p_{perm} = 0.003; *SI Appendix*, Fig. S2). This unimodal/heteromodal distinction replicated in the GSP sample for both RSFA (p_{perm} = 0.001) and GBC (p_{perm} = 0.001). Together, these data provide evidence for subtle yet replicable shifts in cortical anatomy and function linked to both depression and trait levels of negative affect.

In Vivo Depression Imaging Phenotypes Track Ex Vivo Expression of SST Interneuron Markers. The above analyses identify structural and functional cortical correlates of negative affect and lifetime depression history. We use these results as a foundation to characterize the cellular and transcriptional correlates of major depression neuroimaging phenotypes, which could yield insight into the biological bases of the disorder and point toward targets for pharmacological intervention. For instance, brain areas that preferentially express genes related to a psychiatric disorder may be particularly vulnerable to illness progression (38, 39). We begin by interrogating transcriptional markers of SST interneurons, which are a pronounced pathophysiological feature of depression (12, 40). Gene markers of SST interneurons are preferentially expressed in corticostriatal reward circuitry and mPFC in donor tissue from healthy populations (39, 41). Further, *SST* expression is reduced within dorsolateral prefrontal cortex and subgenual mPFC in patients with depression (42, 43), and experimental manipulation of SST neurotransmission in rodents modulates antidepressant behaviors (44) and socioaffective processing (45). Depression linked alterations in the function of GABAergic cells, including SST, may influence signal-to-noise properties of cortex and global measures of connectivity (12, 40), which could be reflected across depression-related shifts in RSFA and GBC.

Here, we test whether gene markers of SST interneurons are preferentially expressed in cortical regions most correlated to a history of major depression. Three canonical gene markers of SST interneurons were analyzed (i.e., *SST*, *CORT*, *NPY*; see *SI Appendix*, Fig. S3 for validation), using postmortem cortical Allen Human Brain Atlas (AHBA) data from six healthy adult individuals (see *Methods*). SST-expressing GABAergic interneurons are denoted as "SST interneurons." We note that the three SST markers are not independent of one another. Rather, the analysis of multiple markers reduces reliance on a single transcriptional probe and provides convergent tests of the relationship between SST marker expression and imaging correlates of depression. Normalized expression of *SST*, *CORT*, and *NPY* is displayed across 200 cortical parcels (Fig. 2*A*; see *SI Appendix*, Fig. S4 for bihemispheric maps), and were also summarized across 68 Desikan atlas parcels in order to match ENIGMA structural neuroimaging data.

Across all datasets and modalities, ex vivo expression of SST gene markers spatially correlated to in vivo cortical phenotypes of depression (Fig. 2 *B–E*). That is, *SST*, *CORT*, and *NPY* were expressed most in anterior cortical areas where depression-linked cortical thinning was greatest, an effect that is consistent in both UKB (r_{sst} = −0.25, r_{cort} = −0.22, r_{npy} = −0.31, $ps_{spin} \leq 0.001$) and ENIGMA data (r_{sst} = −0.58, r_{cort} = −0.58, r_{npy} = −0.35, $ps_{spin} \leq 0.004$). In Fig. 2 *B–E*, each point in the dot plot is a cortical parcel. Significance was established using spin-based permutations to account for spatial autocorrelation. As an added test, the strength of the association was benchmarked against permuted gene triplets drawn from a pool of 17,448 brain-expressed AHBA genes (two-sided P value). Results were robust to alternative permutation strategies using sets of cell gene markers (*SI Appendix*, Fig. S4). In terms of function, depression-linked increases in RSFA were greatest in areas with higher relative SST marker expression, across both the UKB (r_{sst} = 0.38, r_{cort} = 0.47, r_{npy} = 0.26, ps_{spin} = 1e-4) and GSP (r_{sst} = 0.18; r_{cort} = 0.24; r_{npy} = 0.22, $ps_{spin} \leq 0.002$) samples. For functional connectivity, SST triplet gene markers were significantly correlated with depression decreases in GBC across data from the UKB (r_{sst} = −0.40, r_{cort} = −0.33, r_{npy} = −0.40, $ps_{spin} \leq$ 1e-4) and the GSP (r_{sst} = −0.30, r_{cort} = −0.39, ps_{spin} < 1e-4; r_{npy} = −0.10, p_{spin} = 0.09). Last, we contextualize SST marker expression within broad gene expression gradients across cortex (Fig. 2*F*) (46). Principal components analysis of the normalized AHBA expression matrix revealed a primary gradient of gene expression that was strongly coupled to both SST marker expression and in vivo correlates of depression. We note that expression of SST markers is not a direct measure of cell abundance and, instead, is likely influenced by a

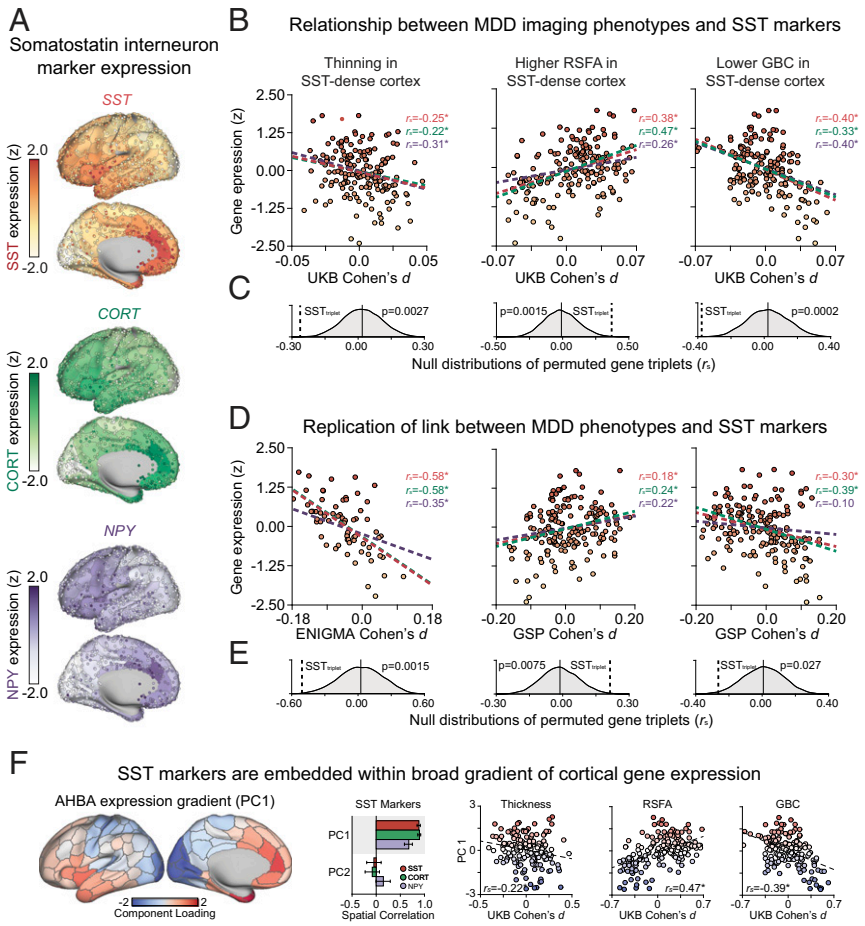

Fig. 2. SST marker genes are spatially associated to in vivo imaging correlates of depression. (*A*) Normalized AHBA cortical expression of three gene markers for SST interneurons: SST (*SST*), cortistatin (*CORT*), and neuropeptide Y (*NPY*). Each dot on the cortical surface represents expression in a single AHBA tissue sample, which is averaged across 200 bihemispheric cortical parcels. (*B*) SST marker expression is spatially correlated with depression-related shifts in cortical thickness (r_{avg} = −0.25), RSFA (r_{avg} = 0.37), and GBC (r_{avg} = −0.38) in UKB data. Circles in the dot plots are cortical parcels, colored by relative *SST* expression. (*C*) Permutation analyses revealed that the strength of the spatial association was greater than what is expected by random selection of 10,000 triplets of brain-expressed genes, as well alternative permutation strategies (*SI Appendix*, Fig. S4). (*D* and *E*) SST marker spatial associations are consistent in replication data for cortical thickness (r_{avg} = −0.51), RSFA (r_{avg} = 0.21), and GBC (r_{avg} = −0.26). SST_{mark} denotes average of *SST*, *NPY*, and *CORT* spatial correlations. (*F*) Principal components analysis of AHBA transcriptional data revealed a rostrocaudal gradient of expression, which was spatially correlated to SST gene markers and cortical correlates of depression. *P < 0.05.

combination of cell density and regional variability in cell transcription patterns (47). We also stress that AHBA transcriptional observations are made in a nonclinical sample, and these analyses do not establish SST interneuron abnormalities in depression. Rather, these data reliably associate SST gene markers to macroscale depression neuroimaging phenotypes, and support investigation of SST interneurons as a possible target for interventions aimed at cortical regions linked to depression.

Transcriptional Correlates of In Vivo Depression Cortical Phenotypes Capture Patterns of Ex Vivo Gene Down-Regulation in Patients. A growing number of multiscale studies suggest that normative patterns of gene expression (e.g., AHBA) can reveal information

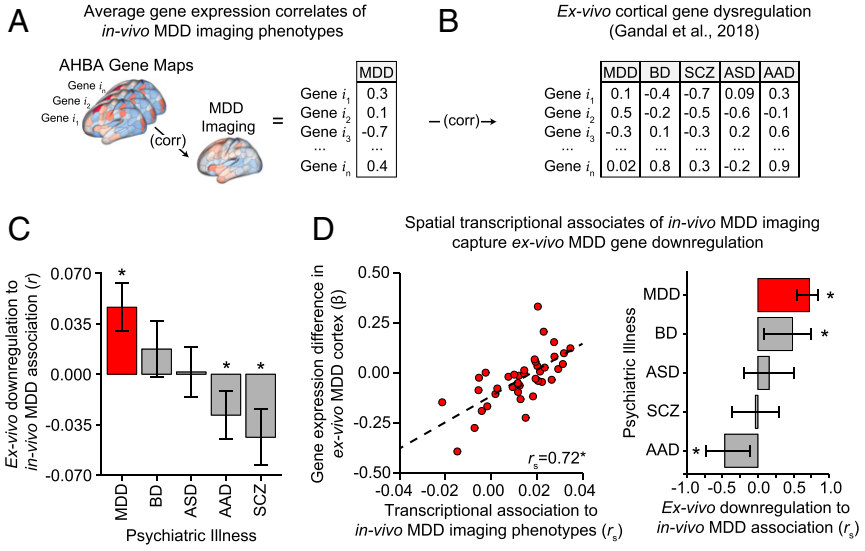

Fig. 3. Association between in vivo depression-linked imaging phenotypes and ex vivo gene dysregulation in depression. (*A*) AHBA spatial gene expression was correlated to each the six depression-linked anatomical and functional neuroimaging maps, then averaged. (*B*) Standardized case–control expression differences were calculated using postmortem metaanalytic data from Gandal et al. (4). (*C*) Average AHBA spatial correlation to depression maps were selectively correlated to postmortem depression down-regulation (r = 0.047, P = 3.4e-8), but not that of other disorders. (*D*) Binned analysis revealed a parallel relationship between gene down-regulation in depression and AHBA correlates of in vivo depression effects (r_s = 0.72, P = 5.3e-7), which was also present for BD (r_s = 0.49, P = 1.7e-3). *P < 0.05. Error bars = 95% CI.

about macroscale brain alterations in psychiatric and neurodevelopmental disorders (38, 39, 48–50). For a given disorder, disease-related changes in cortical function or structure may occur in regions where risk-associated gene sets and molecular processes are most expressed. We test this hypothesis in the context of depression.

Depression-implicated genes were identified using meta-analytic data from Gandal et al. (4), which quantify transcriptional up- or down-regulation in postmortem cortex of patients with depression, bipolar disorder (BD), autism spectrum disorder (ASD), alcohol abuse disorder (AAD), and schizophrenia (SCZ). This results in a gene-wise array for each disorder, where the *i*th entry gives the degree to which the *i*th gene is up- or down-regulated in the diagnostic group (Fig. 3*B*). Postmortem patient tissue is primarily sampled from prefrontal cortex; however, the MDD sample was the only group with samples from ACC (n = 40/83 patient samples; Dataset S1*O*). Reported results are stable if these ACC samples are censored from case–control differential expression analyses.

We tested whether postmortem down-regulated MDD genes are expressed most in cortical regions that are structurally and functionally correlated to depression and negative affect. The cortical AHBA spatial expression of each gene was correlated to each of the six depression-linked structural and functional effect maps detailed above (Fig. 3*A* and Dataset S1 *G–I*). The six spatial correlations for each gene were then averaged to obtain a 1 × 17,448 array reflecting gene-wise spatial association to depression-linked imaging maps. Negative r values indicate stronger association (e.g., increased normative expression in areas of depression-linked cortical thinning).

Ex vivo cortical gene dysregulation in depressed patients was significantly correlated to AHBA transcriptional associates of in vivo depression cortical phenotypes (Fig. 3*A*; r = 0.047, P = 3.4e-8). Suggesting a degree of specificity across diagnostic groups, this positive relationship was selective to ex vivo data from patients with depression and was not present in four comparison psychiatric disorders: SCZ (r = –0.044, P = 1.2e-5), BD (r = –0.017, P = 0.082), ABD (r = –0.028, P = 0.0007), and ASD (r = 0.0015, P = 0.86; Fig. 3*C*). Correlations for each disorder were calculated using all genes that were common across postmortem and AHBA datasets. Of note, SCZ postmortem data showed an effect in the opposite direction, such that SCZ down-regulated genes had lower baseline AHBA expression in depression-implicated cortical areas (e.g., anterior cingulate cortex). This result coincides with reports showing that down-regulated SCZ genes are expressed most in visual, somato/motor, and posterior parietal cortex, which have been implicated in neuroimaging analyses of patients with SCZ (39, 49, 51).

To explore the stability of the observed effects, we conducted a binned analysis relating ex vivo dysregulation to AHBA imaging-expression correlates of depression (Fig. 3*D*). For depression data, the 14,095 analyzable genes that were common across AHBA and Gandal et al. (4) datasets were ranked by ex vivo gene down-regulation and divided into 40 gene bins. Average ex vivo differential expression and average spatial association to in vivo depression phenotypes were calculated for each bin, and then correlated. This approach revealed a significant correlation for depression data (r_s = 0.72, P = 5.3e-7) that was highly stable across choices of bin numbers, ranging from 10 to 40 in increments of 5 (range = 0.69 to 0.92, M = 0.78). The increased magnitude of this correlation (Fig. 3*C*) is likely due to reductions in noise from binned estimates relative to single-gene values. We also observed a significant effect for BD (r_s = 0.49, P = 1.7e-3), but not other disorders. Together, these data indicate that areas marked by expression of genes that are down-regulated in postmortem patient tissue samples are more likely to be anatomically and functionally correlated to depression in vivo (i.e., decreased thickness, decreased GBC, increased RSFA).

Cell Associates of In Vivo Imaging Phenotypes. Given that the pathophysiology of depression is complex and involves interactions among diverse cell classes (25), it is important to characterize the cell transcriptional correlates of depression imaging phenotypes. Using single-cell expression data and gene enrichment techniques, the following analyses accomplish two goals: 1) identify cell types expressing genes correlated to depression cortical imaging phenotypes and 2) identify cell types enriched for gene down-regulation in postmortem cortex of depressed individuals. A polygenic approach was adopted, since not all cell types express highly specific markers of their identity (e.g., *SST* in SST interneurons). Cortical single-nucleus droplet-based sequencing (snDrop-seq) data from Lake et al. (52) were analyzed to identify positively differentially expressed genes across 16 transcriptionally defined cell classes, including five interneuron subtypes (i.e., SST, In1, In3, In4, and In6), five excitatory neuron subtypes (i.e., Ex1, Ex3, Ex4, Ex5, and Ex8), and six nonneuronal subtypes (astrocytes, oligodendrocytes, pericytes, endothelial, microglia, and oligodendrocyte precursor cells [OPC]; see *Methods*). This approach resulted in 16 sets of significant cell gene markers (corrected q < 0.05; Dataset S1*J*). We note that single-cell data from Lake et al. (52) reflect preferential capture

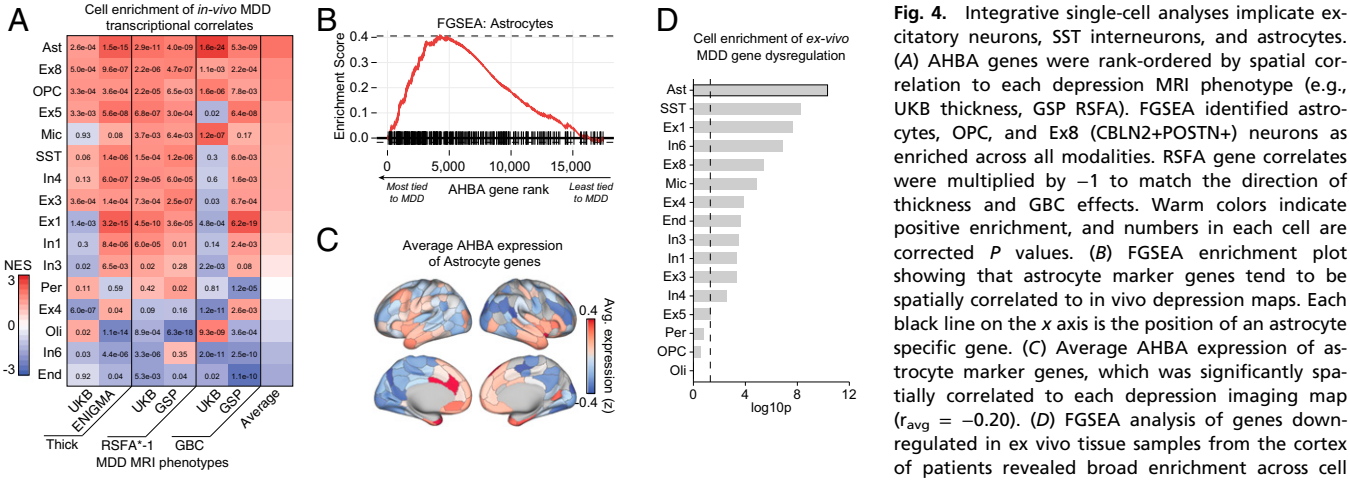

Fig. 4. Integrative single-cell analyses implicate excitatory neurons, SST interneurons, and astrocytes. (*A*) AHBA genes were rank-ordered by spatial correlation to each depression MRI phenotype (e.g., UKB thickness, GSP RSFA). FGSEA identified astrocytes, OPC, and Ex8 (CBLN2+POSTN+) neurons as enriched across all modalities. RSFA gene correlates were multiplied by −1 to match the direction of thickness and GBC effects. Warm colors indicate positive enrichment, and numbers in each cell are corrected P values. (*B*) FGSEA enrichment plot showing that astrocyte marker genes tend to be spatially correlated to in vivo depression maps. Each black line on the x axis is the position of an astrocyte specific gene. (*C*) Average AHBA expression of astrocyte marker genes, which was significantly spatially correlated to each depression imaging map (r_{avg} = –0.20). (*D*) FGSEA analysis of genes down-regulated in ex vivo tissue samples from the cortex of patients revealed broad enrichment across cell classes, that was most pronounced in astrocytes and SST interneurons.

of neuronal over nonneuronal cell types, which may bias the definition of cell specific transcriptional signatures.

Fast-preranked Gene Set Enrichment Analyses (FGSEA) tested whether normative AHBA expression of cell gene markers was significantly more spatially correlated than chance to anatomical and functional imaging markers of depression. Enrichment scores were adjusted for the number of genes in a given cell-type set (i.e., normalized enrichment score [NES]; Dataset S1*K*) (53). Across all six imaging modalities and datasets, astrocytes, OPC, and Ex8 (*CBLN2+POSTN+*) excitatory neurons were significantly enriched for genes correlated to the depression-linked neuroimaging (Fig. 4*A*). In line with a priori hypothesis-driven analyses in Fig. 2, SST interneurons were also positively enriched across four of the six imaging modalities ($q < 0.05$). Astrocyte-specific genes showed the strongest spatial association to depression neuroimaging effects (Fig. 4*A*) and were expressed most within mPFC, anterior temporal lobes, and insular cortex (Fig. 4*C*). The pattern of cell enrichment revealed by FGSEA was stable when compared to an alternative method, where the cortical expression of cell-specific genes was averaged using AHBA data (Fig. 4*C*). For instance, Fig. 4*C* shows the average AHBA expression of the 346 significant astrocyte gene markers. Averaged AHBA cell expression maps for all 16 cell types were then correlated to each of the six depression imaging maps. There was strong cell-wise correspondence between this method and FGSEA ($r_s = 0.92$, $P < 2.2e\text{-}16$). We also conducted a further technical replication of results using polygenic cell deconvolution (*SI Appendix*, Fig. S8) (54). Deconvolution-derived imputed distributions of SST interneurons and astrocytes were the two most spatially correlated cell types across all six modalities ($r_{sst} = -0.26$, $r_{ast} = -0.18$).

The above results identify spatial cell correlates of depression-relevant neuroimaging phenotypes. However, any given cell class might be unchanged in depression or exhibit patterns of gene dysregulation. To address this, we conducted parallel FGSEA analyses using the postmortem data from Gandal et al. (4) to identify cells enriched for gene down-regulation in ex vivo cortical tissue samples from patients with depression (Fig. 4*D*). The NES values were above zero for most cells, indicating a broad pattern of depression-linked down-regulation among nearly all cell markers (Dataset S1*L*). The degree of observed cell enrichment was greatest for SST interneurons (NES = 1.97, $P = 2.5e\text{-}09$) and astrocytes (NES = 1.97, $P = 8.2e\text{-}11$). However, reduced astrocyte transcription was not a global feature of psychiatric illness, such that astrocyte markers showed significantly increased expression in SCZ (NES = −3.34), BP (NES = −3.10), and ASD (NES = −2.09) ex vivo data. Taken together, these findings reveal patterns of reduced cell-specific gene expression in cortex of MDD patients that are greatest for SST interneurons and astrocytes.

Cell-related abnormalities in MDD may reflect inherited genetic risk among cell-preferential pathways, or arise through environmental or second-order effects. Using GWAS data from Wray et al. (3), we examined whether polygenic risk for depression is enriched among cell-preferential genes (Dataset S1*M*). Enrichment was measured with two methods, MAGMA (multi-marker analysis of GenoMic annotation) gene set property analysis (55) and LDSC (linkage disequilibrium score regression) partitioned heritability (56). Single-cell expression data provided transcriptional signatures of eight cell classes, measured from visual cortex (V1C) and dorsal frontal cortex (DFC) (52), as well as replication data from temporal gyrus (MTG) (57). Using LDSC, we observed significant enrichment of polygenic depression risk among interneuron specific genes in DFC ($q = 0.037$) and MTG ($q = 0.046$; Fig. 5, *Left*). MAGMA revealed a similar pattern of enrichment for interneurons that was consistent across all three brain areas (V1C, $q = 1.4e\text{-}4$; DFC, $q = 1.08e\text{-}3$; MTG, $q = 3.4e\text{-}6$). Excitatory neuron enrichment for depression GWAS signal was present with MAGMA, but not LDSC. We did not observe polygenic enrichment among any nonneuronal support cells, despite consistent associations of astrocytes to both in vivo and ex vivo depression phenotypes (Fig. 4).

Gene Ontology of the Transcriptional Associates of Depression Neuroimaging. We next characterize whether transcriptional associates of depression imaging phenotypes capture clinically relevant information, such as sensitivity to a particular class of neurotransmitters, or increased importance of specific signaling pathways. Matching prior approaches (24, 46), gene enrichment analyses were conducted using the top decile of genes correlated to neuroimaging markers of depression ($n = 1{,}745$; Fig. 6 and Dataset S1*N*). The top depression-linked gene decile possessed the greatest number of enrichment terms across molecular function, cellular component, and biological process ontological categories (Fig. 6*A*). Further, genes related to "Depressive Disorder" and "Mental Depression" showed the strongest overlap with the top 10% of neuroimaging MDD gene correlates (Fig. 6*B*). These effects indicate that coherent molecular processes are associated with macroscale brain correlates of MDD.

Consistent with evidence of decreased glutamate and glutamine in the mPFC of patients with depression (22), genes tied to glutamatergic receptors (GO:0008066, $q = 0.004$) and secretion (GO:0014047, $q = 0.013$) were significantly overrepresented in the top decile. We also observed enrichment terms for GABA receptor complex (GO:1902710, $q = 0.029$) and GABAergic synaptic transmission (GO:0051932, $q = 0.041$), in line with prior reports of reduced cortical GABA in patients with depression (58). Major monoamine neurotransmitter systems were also enriched, driven by genes tied to dopamine (GO:0014046; $q = 0.0098$),

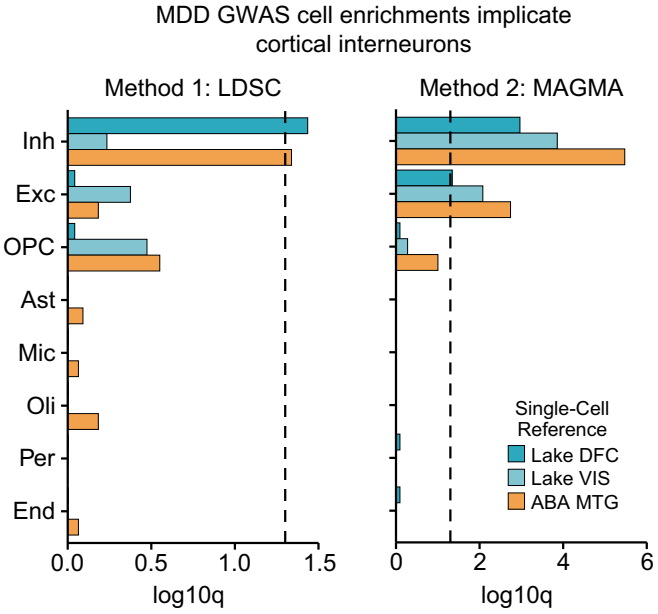

Fig. 5. Genome-wide risk for depression is primarily enriched for inhibitory interneurons, but not glia. Polygenic cell enrichment analyses were conducted across the eight superordinate cell categories across two methods, (*Left*) LDSC and (*Right*) MAGMA. Cell-specific genes are defined using data from the MTG, DFC, and V1C. For LDSC, inhibitory interneuron markers show increased polygenic risk for depression (3). For MAGMA, inhibitory and excitatory genes show enrichment for polygenic depression risk, but the effect is limited to differentially expressed genes defined from the MTG. Dashed line reflects false-discovery rate corrected $P < 0.05$. Inh, inhibitory; Exc, excitatory; Ast, astrocytes; Mic, microglia; Oli, oligodendrocytes; Per, pericytes; End, endothelial.

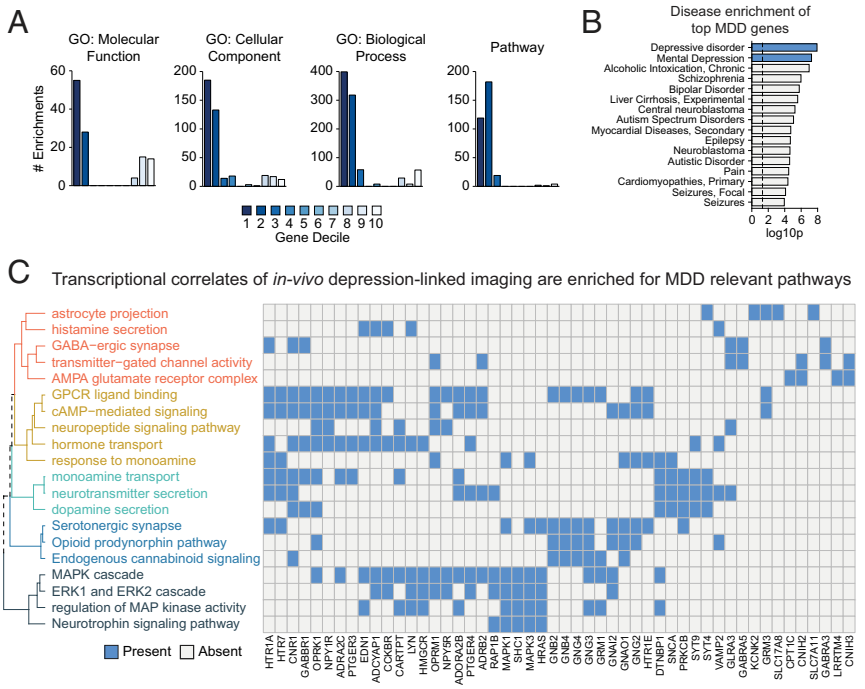

Fig. 6. Transcriptional correlates of in vivo depression-linked imaging phenotypes are enriched for depression-relevant pathways. (*A*) Genes were rank-ordered by average spatial correlation to depression imaging maps, then split into deciles. The top gene deciles had the greatest number of enrichment terms across ontological categories. (*B*) The top gene decile was enriched for depression and other psychiatric disorders. (*C*) Subset of significant enrichment terms for the top decile of MDD imaging correlated genes. Hierarchical clustering is based on overlap of genes in each category. Blue indicates that the gene is included in a given enrichment term. Full enrichment terms are available in Dataset S1.

histamine secretion (GO:0001821, q = 0.036), and serotonergic synapses (Pathway 525336, q = 0.017). Finally, our analyses identified terms related to g protein-coupled second messenger systems (GPCR; Pathway 1269544, q = 0.00059) and downstream intracellular signaling pathways, including to cAMP-mediated signaling (GO:0019933, q = 0.00033), ERK1 and ERK2 cascade (GO:0070371, q = 0.043), MAPK cascade (GO:0000165, q = 0.017), and noncanonical Wnt signaling pathways (GO:0035567, q = 0.0044). These GPCR-activated intracellular cascades are important mediators of the neuromodulatory effects of neuropeptides (59), which were also enriched in our data (GO:0007218, q = 0.00021). Beyond *SST*, the neuropeptides substance P (*TAC1*), cholecystokinin (*CCK*), cocaine-and-amphetamine related transcript (*CARTPT*), galanin (*GAL*), and receptors for mu and kappa opioids (*OPRM1*, *OPRK1*) were in the top decile of MDD correlated genes. The above results provide high-level context about which genes are preferentially expressed within depression-implicated cortex, but should be interpreted with caution since they do not demonstrate that these systems are necessarily altered in patient populations.

These data are also consistent with gene networks implicated in depression from prior independent analyses of postmortem cortical tissue. Specifically, there was strong spatial correlation between all depression imaging maps and the cortical expression of *DUSP6* (r_{avg} = −0.365, 240th/17,448 = 0.003), which inhibits the ERK pathway and is a key hub gene that is down-regulated within the mPFC of patients with depression (5). Depression-linked neuroimaging effects were similarly correlated to *EMX1* expression, which is up-regulated in the mPFC of patient populations. However, these spatial effects were in the opposite direction (r_{avg} = 0.337, 17,034th/17,448 = 0.976), such that normative *EMX1* expression was lower in depression-implicated areas of cortex (e.g., thinning of mPFC; *SI Appendix*, Fig. S7). These findings suggest that expression differences in the cortical territories tied to depression may reflect divergence from normative patterns of area-specific expression, but more data are required to test this hypothesis.

Discussion

The present analyses reveal converging biological signatures of depression that link neuroimaging, cellular, and molecular associates of the illness. Analyses of three population-imaging datasets identified replicable anatomical and functional cortical correlates of depression and negative affect. The observed neuroimaging markers of depression were spatially coupled to patterns of whole-cortex gene expression that were stable across imaging modalities and datasets. Gene associates of in vivo depression cortical phenotypes were correlated with ex vivo patterns of gene down-regulation in cortex of patients with depression, but not samples from other comparison psychiatric disorders. In particular, gene markers of SST interneurons and astrocytes were consistently spatially correlated to in vivo depression neuroimaging effects, and were down-regulated within ex vivo cortical samples from patients with depression. Indicating that some cell classes may be preferentially sensitive to inherited disease risk, cell enrichment analysis of depression GWAS data revealed increased polygenic burden among interneuron-specific genes, but not those of glia. Overall, we identify regionally variable imaging correlates of depression and present cross-modal data highlighting the particular role of SST interneurons and astrocytes. These results suggest potential biological targets for intervention and identify molecular pathways with exaggerated expression in depression-implicated aspects of the cortex.

Our findings have important implications for understanding the cell associates of structural and functional neuroimaging correlates of depression. Prior neuroimaging research reveals subtle patterns of cortical thinning in mPFC, sgACC, and ventral temporal lobes that track illness severity (8, 18, 19). In terms of function, depression is associated with reductions in GBC in mPFC and sgACC (60), that extend to distributed aspects of multimodal association cortex (61). The cellular bases of these alterations remain ambiguous, but may relate to GABAergic alterations (62) or reduced size and density of neurons and glia (7, 26, 63), particularly astrocytes (13). Here, polygenic signatures of astrocytes were consistently associated with depression relevant shifts in both in vivo imaging phenotypes and ex vivo profiles of gene down-regulation (Fig. 4). Astrocytes influence

synapse formation and elimination, and modulate neuronal communication, in part, through glutamate release and NMDAR receptor activation (64, 65). Accordingly, depression-related abnormalities in astrocytes may be involved in reduced glutamate levels in PFC and ACC of patients (13). We did not find evidence for enriched depression polygenic risk among astrocyte-specific genes (Fig. 5); although speculative, this may suggest that observed cell alterations arise through environmental factors not directly tied to genetic risk. For instance, astrocytes are involved in neuroinflammatory signaling and are sensitive to cytokines, which are also implicated in depression etiology (13, 23).

Converging evidence indicates a preferential vulnerability of SST interneurons in depression and affective illness (12, 42). Multiscale studies in humans link SST-related transcription to reward-related corticostriatal circuitry as well as regional variation in cortical function (39, 41). Here, polygenic SST marker genes were significantly spatially correlated to all six depression neuroimaging phenotypes (Fig. 2). That is, SST gene markers were expressed most in sgACC, mPFC, anterior insula, and temporal lobes (Fig. 2) corresponding to areas of depression-linked cortical thinning, increased amplitude, and decreased global connectivity (Fig. 1). Highlighting the association of SST and astrocytes reported here, recent evidence indicates that astrocytes are particularly sensitive to SST interneuron activity, mediated, in part, by binding of SST to astrocytic $GABA_BR$ receptors (66, 67).

In depression, SST-related expression is consistently down-regulated within the sgACC (subgenual anterior cingulate cortex) and amygdala of patients (27, 68). Modulation of SST interneuron activity experimentally reduces depressive-like behavior in animal models of depression (44), and is selectively tied to affective state discrimination in rodents (45). Given evidence that SST expression is sensitive to brain derived neurotrophic factor (BDNF) and is cAMP dependent, depression-related decreases in *SST* may reflect differences in neuronal activity rather than altered cell morphology or number (69, 70). Spatial maps of *SST* marker expression shown here should not be conflated with a direct measure of SST cell density. However, rhesus macaque data indicate that the density of *CALB1* expressing interneurons (a subset of SST cells) and ratio of glia/neurons are highest within agranular limbic cortex relative to lateral PFC (71), consistent with data in rodents (72). Nonetheless, differences in relative expression of the neuropeptides like *SST* and *NPY* are likely functionally important, given their ability to influence neuronal and glial function (59, 66). Increased relative expression of *SST* has further been documented among distributed whole-brain affective circuitry, including the nucleus accumbens, ventral tegmental area, mediodorsal thalamus, and anterior hippocampus (39, 72, 73). We also found that cortical SST marker expression was embedded within a broader rostrocaudal gradient of gene transcription (Fig. 2*F*), which may be a biologically meaningful feature related to hierarchical organization of cortex (39, 46, 72, 74). Future work should investigate whether alterations in SST cells in depression are consistent across distributed corticolimbic circuitry.

Our results suggest that normative patterns of brain gene expression capture biologically meaningful information about in vivo depression-related differences in cortex. These data converge with reports that spatial gene expression may reflect regional sensitivity to psychiatric illnesses (39, 75), neurodevelopmental disorders (38), and normative brain function and organization (41, 76, 77). Here, we demonstrate that spatial transcriptional correlates of depression imaging phenotypes correlated with gene down-regulation in postmortem patient tissue samples (Fig. 3). Interestingly, the transcriptional signatures of depression neuroimaging effects showed a negative correlation to gene down-regulation in AAD. Despite evidence for positive genetic correlation between the two disorders (78), this result is consistent with data showing preferential disruption of glial cells in depression, relative to noncomorbid alcohol abuse (79). Given that postmortem transcriptional data necessarily reflect illness end points, differences in brain gene expression among genetically related disorders could be due to varying behavioral, environmental, and medication-related factors. Overall, our findings support the emerging hypothesis of "transcriptional vulnerability" (38, 49–51), where brain regions with high baseline expression of disorder-linked genes are more likely to be affected over the course of an illness. The current results point toward specific receptors and signaling pathways with increased expression in depression-implicated brain areas, which may guide targets for biological interventions. Although a subset of our data include healthy young adults with varying levels of negative affect (32), the current analyses largely reflect neuroimaging and transcriptional correlates at the depressive illness end points, and neurodevelopmental approaches are required to prospectively identify vulnerable brain regions and networks.

Our in vivo analyses identified consistent, yet subtle, anatomical and functional correlates of MDD and trait negative affect (Fig. 1). The small effect sizes observed in UKB data could be due to the relatively older mean age of our sample or the use of self-report MDD symptoms (see *SI Appendix*, Fig. S1 for validation of MDD phenotype). However, null hypothesis significance testing becomes problematic when analyzing very large samples, particularly in the UKB, which has a target recruitment of 100,000 individuals (80). For instance, the magnitude of linear effects linking brain features and behavior tend to be muted and generally require multivariate techniques to account for an appreciable amount of variance (31), possibly reflecting the distributed nature of information processing in the brain (81). Such a scenario echoes issues faced within the field of population genetics, where single genetic polymorphisms may have fleetingly small effects, but global or whole-genome analyses explain a considerable portion of trait variance (82). Future work should investigate whether the pattern and magnitude of disease-relevant neuroimaging effects vary by patient subpopulation or are differentially expressed across divergent symptom presentations (5) or diagnosis constructs (83), particularly given marked symptom heterogeneity seen in patients with depression.

The current study should be interpreted in light of several limitations, including our focus on cortical relative to subcortical brain correlates of MDD. In addition to cortical abnormalities, history of depressive illness has been linked to structural abnormalities in hippocampus and amygdala (84, 85), as well as functional alterations in striatal circuitry (86). Additional research is needed to bridge these subcortical features of depression with underlying transcriptional abnormalities. Further, our cell enrichment analyses of MDD polygenic liability were also conservative, such that we only examined broad cell classes (e.g., inhibitory interneurons, oligodendrocytes). More fine-grained analyses of cell subtypes (e.g., SST interneurons, PVALB interneurons) should be prioritized, as statistical power increases for both GWAS and single-cell transcriptomics. Finally, the depressive phenotype in the UKB sample reflected lifetime history of depression rather than symptom presentations concurrent with the MRI scan. Although we show consistency across multiple phenotypes and datasets (Fig. 1), more detailed assessment of individual symptoms may identify anatomical and functional neural correlates of depressive subphenotypes (10).

A strength of the current analyses is our focus on global patterns of brain anatomy and function. For instance, our whole-cortex analyses revealed a surprising pattern of slightly increased visual cortex thickness in patients relative to controls (Fig. 1), an effect that may be missed by small samples or hypothesis-driven examinations of select brain areas. Of interest, this anatomical

effect may, at least in part, explain patterns of increased functional connectivity in occipital cortex, reported both here and through other collection efforts (83). We also find that MDD and trait negative affect were associated with distributed functional changes that dissociate unimodal versus heteromodal cortex (*SI Appendix*, Fig. S2). GBC was reduced in MDD across orbitofrontal cortex (OFC), mPFC, and anterior temporal lobes, which contrasts increased GBC within visual cortex. These data support previous reports on smaller samples of reduced GBC in mPFC (60, 87), but highlight the presence of broad spatially cohesive patterns of connectivity change. In this study, resting-state functional amplitude (RSFA) was increased in depression within heteromodal cortex, but was reduced in unimodal regions (Fig. 1). It is important to note that RSFA reflects vascular as well as neural factors (88), although growing evidence suggests that the blood oxygen level-dependent (BOLD) signal variability is robust to cerebrovascular nuisance correction (89), related to between-subjects behavioral variation (90), and is characterized by heritable interindividual variance that is enriched for interneuron-associated genes (39). Depression changes in RSFA and GBC were spatially anticorrelated to one another, supporting prior evidence that BOLD signal amplitude is predictive of within-subject change in functional connectivity (90). In sum, these data identify spatially variable functional patterns across cortex in depression and negative affect, providing a neuroimaging foothold from which to interrogate underlying molecular and cellular associates.

Conclusion

In this study, we identify replicable anatomical and functional neuroimaging correlates of depression and trait negative affect, which serve as a foundation for integrative genetic analyses. Normative expression of polygenic SST interneuron markers in cortex were significantly spatially associated with depression correlates across all imaging modalities and datasets, in line with the hypothesized importance of this cell type in the disorder. Our data also suggest that the transcriptional associates of depression neuroimaging phenotypes capture global patterns of differential gene expression in depression, measured in ex vivo patient cortical tissue. Incorporation of single-cell gene expression data showed that gene markers of SST interneurons and astrocytes were particularly strong spatial associates of depression imaging phenotypes, and were preferentially down-regulated in postmortem tissue samples from patient populations. Enrichment analyses of depression transcriptional associates identified multiple biological pathways, including neuropeptides, GPCR binding, and related intracellular MAPK, ERK, and cAMP signaling. Together, these data provide an integrative profile of the biology of depression that spans neuroscientific levels of analysis, connecting specific genes, cell classes, and molecular pathways to in vivo imaging correlates of illness.

Methods

Major Depressive Phenotypes.

UKB. Lifetime history of depression was measured from self-report questions collected during the imaging scan visit. MDD definitions followed methods of Smith et al. (91). Individuals meeting criteria for single-episode, moderate recurrent, or severe recurrent depression reported having had a period of depressed mood or anhedonia for a week or more (UKB Fields: 4598/4631), with the longest period of anhedonia/depressed mood lasting two or more weeks (UKB Fields: 4609/5375). Single-episode depression was characterized by endorsement of only one lifetime symptomatic period (UKB Fields: 4620/5386) and treatment seeking with a general practitioner (GP) or psychiatrist (UKB Fields: 2090/2100). Both moderate recurrent and severe recurrent depressive diagnoses required two or more lifetime symptomatic episodes of anhedonia or depressed mood. Assignment of moderate recurrent depression required treatment seeking through a GP, but not a psychiatrist, whereas assignment of severe recurrent depression required the opposite. Classifications of single-episode, moderate recurrent, and severe recurrent depression were mutually exclusive. However, moderate and severe depression were reclassified into a binary indicator, and data from individuals with a single lifetime episode of depression were not analyzed. Due to the retrospective self-report nature of symptom inventories, participants endorsing a single episode of MDD were excluded in an effort to reduce the rate of false positives.

ENIGMA. The results from the ENIGMA metaanalytic study by Schmaal et al. (8) were used for comparison against UKB anatomical effects. Cortical thickness changes in recurrent adult depression versus controls were analyzed, and quantified as Cohen's *d* across 68 Desikan atlas regions of interest (ROIs). Sample size varied by ROI: MDD patients (n = 1,206 to 1,302; female = 61.69%) and control participants (n = 7,350 to 7,450; female = 52.64%). Metaanalytic estimates controlled for sex, age, and scan center. The weighted mean age of ENIGMA controls was 54.57 y (SD = 12.88), compared to the mean age of 44.75 y (SD = 12.02) for MDD patients. Additional information about patient and study demographics are published (8).

GSP. Trait negative affect was assessed in the same manner as used by Holmes et al. (20). A single self-report measure comprised five scales related to history of negative emotion, including the NEO (neuroticism, extraversion, openness) neuroticism scale (92), the behavioral inhibition scale from the BIS/BAS (Behavioral Inhibition System/Behavioral Approach System) (93), reported mood disturbance assessed with the Profile of Mood State (94), the Spielberger State/Trait Anxiety Inventory (95), and measures of harm avoidance assessed with the Temperament and Character Inventory (96). Scores on each scale were z-transformed across individuals prior to averaging to generate a trait negative affect composite score.

Neuroimaging Processing.

UKB. Structural and functional MRI data from the UKB were analyzed using an extended version of the standard UKB preprocessing pipeline (https://git.fmrib.ox.ac.uk/falmagro/UK_biobank_pipeline_v_1). Anatomical and functional data from 16,350 individuals were available for analysis after preprocessing (Project ID: 25163). Data were collected on Siemens 3T Skyra and 32-channel receive head coil. T1-weighted structural scans were reconstructed from raw DICOMS (Digital Imaging and Communications in Medicine) (TR = 2,000 ms, TE = 2.01 ms, TI = 880 ms, flip angle = 8°, resolution = 1 mm^3). Minimally preprocessed resting-state functional MRI scans were acquired using a multiband gradient echo echo planar imaging (EPI) sequence (length = 6 min, field of view [FOV] = 210 mm, slices = 64, TR = 735 ms, TE = 39 ms, resolution = 2.4 mm^3), collected on multiple scanners across imaging centers in Cheadle and Newcastle, United Kingdom. Detailed imaging protocols are published (31). Scans were not analyzed if they were marked as corrupted or "unusable" by UKB automated quality control tools. See *SI Appendix* for details of our surface-based resting-state preprocessing.

Parcellated surface-based estimates of RSFA (SD of BOLD time series) and functional connectivity were estimated using HCP (Human Connectome Project) workbench. RSFA values were z-transformed within individuals. A subject's 200 × 200 functional connectivity estimates were Fisher Z-transformed. GBC was calculated as the average correlation of a given cortical parcel to all 199 other parcels. Quantitative quality control included row-wise deletion for missing thickness and resting-state estimates across the 200 cortical parcels. Individuals with average cortical thickness, RSFA, or GBC more than ±3 SD from the mean were removed. Similarly, we identified outliers at the level of individual parcels, and individuals with thickness, RSFA, or GBC outliers in more than 5% of all cortical parcels were removed. Finally, individuals with outlier (±3 SD) total brain size or white matter lesion volume were censored from further analyses. MDD case status was binarized to identify controls and individuals with moderate/severe recurrent lifetime history of depression. Individuals reporting only a single lifetime history of MDD were not analyzed. The final sample included (n = 2,136) cases and (n = 12,084) controls (age: 62.78 ± 7.40 y; percent female = 53.07).

GSP. Neuroimaging and phenotypic data from the open-access GSP were obtained (https://dataverse.harvard.edu/dataverse/GSP) (32). All individuals were healthy young adults of White/non-Hispanic ancestry with no history of psychiatric illness. Imaging data were acquired across multiple Seimens Tim Trio scanners at Massachusetts General Hospital and Harvard University. Only data from individuals scanned using 12-channel phased array head coils were analyzed. Anatomical data were collected using a multiecho T1w magnetization-prepared gradient-echo image (multiecho MPRAGE; TR = 2,200 ms; TI = 1,100 ms; TE = 1.54 ms; FA = 7°; 1.2 mm^3; FOV = 230). T2w anatomical data were acquired in the same session using a turbo spin echo with high sampling efficiency [multiecho MPRAGE (97): TR = 2,800 ms; TE = 327 ms; 1.2 mm^3; FOV = 192], with a bandwidth matched to the T1w acquisition (652 Hz per pixel). Resting-state functional MRI data were acquired using a single 6-min gradient EPI sequence (TR = 3,000 ms; TE = 30 ms;

FA = 85°; 3 mm^3, FOV = 216; slices = 47; interleaved foot-head acquisition = 1, 3, . . .45, 47, 2, 4, . . ., 44, 46).

Behavioral and neuroimaging quality control resulted in 947 individuals for subsequent analyses (age: 18 y to 74 y, M = 21.8 ± 5.05; percent female: 54.38; Shipley IQ: 113.40 ± 8.49). Individuals with missing GBC or RSFA data in any cortical parcel were not analyzed. We then identified individuals possessing GBC or RSFA outliers (±3 SD) in greater than 5% of cortical parcels, or extreme outliers in global GBC or RSFA (±4 SD). RSFA values were then z transformed within individuals. See *SI Appendix* for full details of resting-state preprocessing.

Regression Linking Depressive Phenotypes to Neuroimaging. Regression analyses were conducted independently across the 200 bihemispheric cortical parcels. Quantitative variables were z-transformed. In the UKB, the effect of moderate/severe MDD history (0/1) on cortical thickness, RSFA, and GBC were estimated, covarying for sex, age, age^2, age*sex, age^2*sex, total brain size, volume of white matter hyperintensities, self-reported ancestry, genetically estimated ancestry (White/non-Hispanic or not), T1 inverse SNR (signal to noise ratio), MRI run-wise average motion and inverse SNR, diastolic and systolic blood pressure, X/Y/Z position of brain in the scanner (center mass of brain mask), and UKB imaging acquisition center. Regression analyses in the GSP sample were conducted in a parallel fashion to predict RSFA and GBC from trait negative affect, controlling for age, sex, age, age^2, age*sex, age^2*sex, intracranial volume, height, weight, Shipley fluid intelligence, years of education, scanner bay, and scanner console version. Cohen's *d* effect size estimates of depression status were calculated using the t statistic and df (degrees of freedom) from the regression

$$d = \frac{2 * t}{\sqrt{df}}.$$

AHBA. Publicly available human gene expression data from six postmortem donors (one female), aged 24 y to 57 y (42.5 ± 13.38 y) were obtained from the Allen Institute. Probes without Entrez IDs were removed, and probe-wise noise for each donor was quantified as the number of above-threshold samples in cortex, divided by total cortical sample count. A probe-wise average was computed across all six donors, which was used to remove probes expressed in fewer than 20% of cortical samples. If more than one probe existed for a given gene, the one with the highest mean expression was selected for further analysis, resulting in 17,448 brain-expressed genes. All analyses were conducted according to the guidelines of the Yale University Human Subjects Committee

Individual cortical tissue samples were mapped to each AHBA donor's Freesurfer-derived cortical surfaces (98). Native space midthickness surfaces were transformed into a common fsLR32k group space while maintaining the native cortical geometry of each individual donor. The native voxel coordinate of each tissue sample was mapped to the closest surface vertex (99). A cortical tissue sample was not analyzed if it was greater than 4 mm from the nearest surface vertex, resulting in 1,683 analyzable cortical samples. Expression was then averaged across 200 roughly symmetric surface ROIs from the 17-network functional parcellation of Schaefer et al. (34). After removal of parcels that did not overlap with an AHBA cortical sample, 173 ROIs remained for analysis. To allow for comparison to ENIGMA thickness data, gene expression was also summarized according to the 68-parcel Desikan atlas (100). Even after normalization procedures employed by the Allen Institute to correct for batch effects, we observed residual differences in global expression intensity across cortical samples, possibly reflecting technical artifacts. Thus we perform within-sample z-transform normalization, similar to Burt et al. (46), to reduce global expression differences across cortex. Microarray expression of each gene was then mean- and variance-normalized, revealing relative expression differences across cortex. Cortical data visualization was carried out using "*wb_view*" from the HCP workbench.

Single-Cell Transcriptional Enrichment Analyses. We identified transcriptional markers of individual cell types using snDrop-seq UMI (Unique Molecular Identifier) counts for cells from visual (BA17) and dorsal frontal cortex (BA 6/9/10), obtained from Gene Expression Omnibus (GSE97942) (52). UMI processing with Seurat was done separately for visual and frontal samples (101). Initial filtering was conducted to ensure removal of genes expressed in fewer than three cells, as well as cells with fewer than 200 expressed genes. Expression values were normalized for each cell according to total expression values (i.e., "LogNormalize"), as well as covariates for sequencing platform and processing batch. Predefined superordinate cell categories from Lake et al. (52) were used, which identified 16 cell classes that were present in both frontal and visual cortex. Differential expression in each cell type, relative to all others, was calculated using the Wilcoxon rank sum test in Seurat (i.e., "FindMarkers"). Seurat was used to conduct the same preprocessing steps on single-cell RNA sequencing (RNAseq) data from the middle temporal gyrus (MTG) obtained from the Allen Institute (https://portal.brain-map.org/atlases-and-data/rnaseq) (57).

Cell enrichment analyses were conducted using FGSEA (53). Cell-specific genes were identified based on significant positive differential expression in both frontal and visual cortex Lake data (false discovery rate ≤ 0.05). Cell-wise FGSEA was then conducted for each neuroimaging modality (i.e., thickness, RSFA, GBC) and dataset (i.e., UKB, ENIGMA, GSP). Gene transcriptional associates of each imaging phenotype were identified using normalized AHBA expression data. That is, the cortical expression of each gene was spatially correlated to parcel-level depression neuroimaging effects (Cohen's *d*). RSFA values were multiplied by −1 to align the direction of thickness and GBC effects. Ranked gene lists for FGSEA were in descending order based on spatial correlation to depression imaging effects. Enrichment scores are the same as that of GSEA (102). We report NESs that account for the number of genes present in each cell marker group. Single-cell RNAseq MTG data were used as replication data (57). See *SI Appendix* for details on single-cell replication analyses, including imputation of spatial cell density across cortex.

AHBA Spatial Correlation to Depression-Linked Neuroimaging. Normalized AHBA expression data, summarized by surface atlas parcels, was spatially correlated (Spearman's) to each of the six depression-linked neuroimaging phenotypes. We specifically investigate whether gene markers of SST interneurons (*CORT, NPY, SST*) are spatially associated with anatomical and functional correlates of depression. Given spatial autocorrelation among AHBA expression data, the significance of each expression-to-imaging correlation was assessed using spin-based permutation tests, which preserve the proximity-based correlation structure of expression maps (35). We also perform multiple gene-based permutations to benchmark the strength of the association between SST gene markers and each depression-linked imaging phenotype. The first permutation randomly selects gene triplets (n = 10,000 perms) from the pool of 17,445 brain-expressed genes (this excludes *CORT, NPY, SST*). The second selects gene triplets (n = 10,000 perms) from a select pool of 1,609 genes that were identified as significant cell type markers according to single-cell data from Lake et al. (52) (excluding markers of SST interneurons). The third permutation strategy selects genes from the same pool of 1,609 marker genes; however, each triplet is composed of genes that are significant markers for the same cell type (n = 10,000 perms per cell type, excluding markers of SST interneurons). The results of each permutation strategy are presented in *SI Appendix*, Fig. S5.

Ex Vivo Psychiatric Patient Differential Expression. Metaanalytic estimates of differential expression from Gandal et al. (4) were analyzed (https://github.com/mgandal/Shared-molecular-neuropathology-across-major-psychiatric-disorders-parallels-polygenic-overlap). Gene expression values were normalized prior to differential expression calculation with linear mixed effects modeling in order to provide standardized beta coefficients, indicating the degree that a gene is up- or down-regulated for a given psychiatric population. Analyses included cortical expression data from patients with MDD, ASD, BD, AAD, and SCZ. Information about data preprocessing is published (4), and sample information is available in Dataset S1. Gene-wise patient differential expression (i.e., normalized beta) was then correlated to the gene-wise spatial correlation to in vivo neuroimaging phenotypes.

Single-Cell MDD GWAS Enrichment. We tested whether polygenic risk for depression, using the GWAS from Wray et al. (3), was enriched among cell-specific genes. Enrichment was measured using MAGMA gene-set property analysis (55) and LDSC partitioned heritability (103). Cell specificity of gene expression was measured with single-cell data from V1C, DFC, and MTG. Cell-specific expression was quantified using the EWCE (Expression Weighted Celltype Enrichment) R package (104). Genes were split into deciles for each cell, ordered from most specifically expressed to least. LDSC annotation files were created using the 1000 Genomes European Phase 3 release. Cell enrichment estimates were conditional on a baseline model ("1000G_EUR_Phase3_baseline") of 53 genomic regions (enhancer, genic, etc.). Enrichment statistics were reported for the top gene decile for each dataset and cell type. MAGMA gene property analyses followed those of Watanabe et al. (105). We calculated averaged gene expression for each cell type and included overall gene-wise expression, collapsed across all cells, as a covariate. This approach also does not depend upon the creation of gene

bins. For both methods, *P* values were corrected for multiple comparisons (Benjamini–Hochberg) separately for each single-cell dataset (e.g., eight tests for DFC snDrop-seq data).

Gene Ontology Enrichment Analysis. ToppGene (106) was used to identify biological enrichment terms across the MDD gene deciles. Genes were rank-ordered based on their average AHBA spatial correlation, collapsed across the six depression-linked neuroimaging maps, and then split into evenly sized gene deciles. The numbers of enrichment terms for each gene decile were then compared (Fig. 6*A*), split across major ontological categories (Biological Process, Cell Component, etc.). We illustrate specific genes enriched among a circumscribed set of enrichment categories (Fig. 6*C*). Similarity of each enrichment term was defined as the number of overlapping genes between two categories, relative to the number of total genes linked to both enrichment categories. This similarity matrix was then hierarchically clustered to identify clusters of similar enrichment terms. Genes were selected for plotting if they were present among multiple enrichment categories.

Data and Code Availability. Study data are available in the Supplementary Material or through open-access third party sources. Data and code used in this analysis are publicly available upon publication, unless restricted by data use agreement. UKB data are publicly available upon third-party authorization: https://www.ukbiobank.ac.uk/register-apply/. Associated code is publicly available: https://github.com/kevmanderson/2020_PNAS_Depression. Allen Human Brain Atlas is available here: https://human.brain-map.org/. Brainspan data is available here: http://www.psychencode.org/. Post-mortem patient expression data is available here: https://github.com/mgandal/Shared-molecular-neuropathology-across-major-psychiatric-disorders-parallels-polygenic-overlap. Single cell expression data is available at the National Center for Biotechnology Information under the accession code GSE97942. Genomics Superstruct Project data is available by application here: https://dataverse.harvard.edu/dataverse/GSP. Depression GWAS data is available here: https://www.med.unc.edu/pgc/download-results/.

ACKNOWLEDGMENTS. This work was supported by the National Institute of Mental Health (Grants K01MH099232 and R01MH120080 to A.J.H.) and the NSF (Grant DGE-1122492 to K.M.A.). R.K., J.L., T.H., and B.T.T.Y. were supported by Singapore Ministry of Education (MOE) Tier 2 (Grant MOE2014-T2-2-016), National University of Singapore (NUS) Strategic Research (Grant DPRT/944/09/14), NUS School of Medicine Aspiration Fund (Grant R185000271720), Singapore National Medical Research Council (Grant CBRG14nov007), NUS Youth Innovation Award, and by the Singapore National Research Foundation Fellowship (Class of 2017). Any opinions, findings, and conclusions or recommendations expressed in this material are those of the author(s) and do not reflect the views of National Research Foundation, Singapore. Analyses were made possible by the high-performance computing facilities provided through the Yale Center for Research Computing. We thank B. J. Casey, Ty Cannon, Steve Chang, Nick Turk-Browne, Jonathan Warrell, Prashant Emani, and Lauren Patrick for their feedback on early versions of this manuscript. Raw data were provided by the Brain Genomics Superstruct Project of Harvard University and Massachusetts General Hospital, the Allen Institute for Brain Science, and UK Biobank (Project ID 25163).

1. P. F. Sullivan, M. C. Neale, K. S. Kendler, Genetic epidemiology of major depression: Review and meta-analysis. *Am. J. Psychiatry* **157**, 1552–1562 (2000).
2. J. L. Price, W. C. Drevets, Neurocircuitry of mood disorders. *Neuropsychopharmacology* **35**, 192–216 (2010).
3. N. R. Wray *et al*.; eQTLGen; 23andMe; Major Depressive Disorder Working Group of the Psychiatric Genomics Consortium, Genome-wide association analyses identify 44 risk variants and refine the genetic architecture of major depression. *Nat. Genet.* **50**, 668–681 (2018).
4. M. J. Gandal *et al*.; CommonMind Consortium; PsychENCODE Consortium; iPSYCH-BROAD Working Group, Shared molecular neuropathology across major psychiatric disorders parallels polygenic overlap. *Science* **359**, 693–697 (2018).
5. B. Labonté *et al*., Sex-specific transcriptional signatures in human depression. *Nat. Med.* **23**, 1102–1111 (2017).
6. D. Cotter, D. Mackay, S. Landau, R. Kerwin, I. Everall, Reduced glial cell density and neuronal size in the anterior cingulate cortex in major depressive disorder. *Arch. Gen. Psychiatry* **58**, 545–553 (2001).
7. D. Ongür, W. C. Drevets, J. L. Price, Glial reduction in the subgenual prefrontal cortex in mood disorders. *Proc. Natl. Acad. Sci. U.S.A.* **95**, 13290–13295 (1998).
8. L. Schmaal *et al*., Cortical abnormalities in adults and adolescents with major depression based on brain scans from 20 cohorts worldwide in the ENIGMA Major Depressive Disorder Working Group. *Mol. Psychiatry* **22**, 900–909 (2017).
9. R. H. Kaiser, J. R. Andrews-Hanna, T. D. Wager, D. A. Pizzagalli, Large-scale network dysfunction in major depressive disorder: A meta-analysis of resting-state functional connectivity. *JAMA Psychiatry* **72**, 603–611 (2015).
10. A. T. Drysdale *et al*., Resting-state connectivity biomarkers define neurophysiological subtypes of depression. *Nat. Med.* **23**, 28–38 (2017).
11. C. H. Xia *et al*., Linked dimensions of psychopathology and connectivity in functional brain networks. *Nat. Commun.* **9**, 3003 (2018).
12. C. Fee, M. Banasr, E. Sibille, Somatostatin-positive gamma-aminobutyric acid interneuron deficits in depression: Cortical microcircuit and therapeutic perspectives. *Biol. Psychiatry* **82**, 549–559 (2017).
13. G. Rajkowska, C. A. Stockmeier, Astrocyte pathology in major depressive disorder: Insights from human postmortem brain tissue. *Curr. Drug Targets* **14**, 1225–1236 (2013).
14. A. J. Holmes, L. M. Patrick, The myth of optimality in clinical neuroscience. *Trends Cogn. Sci. (Regul. Ed.)* **22**, 241–257 (2018).
15. E. A. Phelps, J. E. LeDoux, Contributions of the amygdala to emotion processing: From animal models to human behavior. *Neuron* **48**, 175–187 (2005).
16. R. Adolphs, The neurobiology of social cognition. *Curr. Opin. Neurobiol.* **11**, 231–239 (2001).
17. H. S. Mayberg, Limbic-cortical dysregulation: A proposed model of depression. *J. Neuropsychiatry Clin. Neurosci.* **9**, 471–481 (1997).
18. W. C. Drevets, J. L. Price, M. L. Furey, Brain structural and functional abnormalities in mood disorders: Implications for neurocircuitry models of depression. *Brain Struct. Funct.* **213**, 93–118 (2008).
19. M. T. Treadway *et al*., Illness progression, recent stress, and morphometry of hippocampal subfields and medial prefrontal cortex in major depression. *Biol. Psychiatry* **77**, 285–294 (2015).
20. A. J. Holmes *et al*., Individual differences in amygdala-medial prefrontal anatomy link negative affect, impaired social functioning, and polygenic depression risk. *J. Neurosci.* **32**, 18087–18100 (2012).
21. L. A. Maglanoc *et al*., Brain connectome mapping of complex human traits and their polygenic architecture using machine learning. *Biol. Psychiatry* **87**, 717–726 (2020).
22. S. Moriguchi *et al*., Glutamatergic neurometabolite levels in major depressive disorder: A systematic review and meta-analysis of proton magnetic resonance spectroscopy studies. *Mol. Psychiatry* **24**, 952–964 (2019).
23. C. L. Raison, L. Capuron, A. H. Miller, Cytokines sing the blues: Inflammation and the pathogenesis of depression. *Trends Immunol.* **27**, 24–31 (2006).
24. M. J. Hawrylycz *et al*., An anatomically comprehensive atlas of the adult human brain transcriptome. *Nature* **489**, 391–399 (2012).
25. H. K. Manji, W. C. Drevets, D. S. Charney, The cellular neurobiology of depression. *Nat. Med.* **7**, 541–547 (2001).
26. G. Rajkowska *et al*., Morphometric evidence for neuronal and glial prefrontal cell pathology in major depression. *Biol. Psychiatry* **45**, 1085–1098 (1999).
27. A. Tripp, R. S. Kota, D. A. Lewis, E. Sibille, Reduced somatostatin in subgenual anterior cingulate cortex in major depression. *Neurobiol. Dis.* **42**, 116–124 (2011).
28. E. Setiawan *et al*., Role of translocator protein density, a marker of neuroinflammation, in the brain during major depressive episodes. *JAMA Psychiatry* **72**, 268–275 (2015).
29. R. C. Shelton *et al*., Altered expression of genes involved in inflammation and apoptosis in frontal cortex in major depression. *Mol. Psychiatry* **16**, 751–762 (2011).
30. J. W. Murrough, C. G. Abdallah, S. J. Mathew, Targeting glutamate signalling in depression: Progress and prospects. *Nat. Rev. Drug Discov.* **16**, 472–486 (2017).
31. K. L. Miller *et al*., Multimodal population brain imaging in the UK Biobank prospective epidemiological study. *Nat. Neurosci.* **19**, 1523–1536 (2016).
32. A. J. Holmes *et al*., Brain Genomics Superstruct Project initial data release with structural, functional, and behavioral measures. *Sci. Data* **2**, 150031 (2015).
33. N. Cai *et al*.; MDD Working Group of the Psychiatric Genomics Consortium, Minimal phenotyping yields genome-wide association signals of low specificity for major depression. *Nat. Genet.* **52**, 437–447 (2020).
34. A. Schaefer *et al*., Local-global parcellation of the human cerebral cortex from intrinsic functional connectivity MRI. *Cereb. Cortex* **28**, 3095–3114 (2018).
35. A. F. Alexander-Bloch *et al*., On testing for spatial correspondence between maps of human brain structure and function. *Neuroimage* **178**, 540–551 (2018).
36. E. M. Gordon *et al*., Generation and evaluation of a cortical area parcellation from resting-state correlations. *Cereb. Cortex* **26**, 288–303 (2016).
37. M. W. Cole, G. Repovš, A. Anticevic, The frontoparietal control system: A central role in mental health. *Neuroscientist* **20**, 652–664 (2014).
38. J. Seidlitz *et al*., Transcriptomic and cellular decoding of regional brain vulnerability to neurogenetic disorders. *Nat. Commun.* **11**, 3358, 10.1038/s41467-020-17051-5 (2020).
39. K. M. Anderson *et al*., Transcriptional and imaging-genetic association of cortical interneurons, brain function, and schizophrenia risk. *Nat. Commun.* **11**, 2889 (2020).
40. R. S. Duman, G. Sanacora, J. H. Krystal, Altered connectivity in depression: GABA and glutamate neurotransmitter deficits and reversal by novel treatments. *Neuron* **102**, 75–90 (2019).
41. K. M. Anderson *et al*., Gene expression links functional networks across cortex and striatum. *Nat. Commun.* **9**, 1428 (2018).
42. M. L. Seney, A. Tripp, S. McCune, D. A. Lewis, E. Sibille, Laminar and cellular analyses of reduced somatostatin gene expression in the subgenual anterior cingulate cortex in major depression. *Neurobiol. Dis.* **73**, 213–219 (2015).
43. E. Sibille, H. M. Morris, R. S. Kota, D. A. Lewis, GABA-related transcripts in the dorsolateral prefrontal cortex in mood disorders. *Int. J. Neuropsychopharmacol.* **14**, 721–734 (2011).

44. T. Fuchs *et al*., Disinhibition of somatostatin-positive GABAergic interneurons results in an anxiolytic and antidepressant-like brain state. *Mol. Psychiatry* **22**, 920–930 (2017).
45. D. Scheggia *et al*., Somatostatin interneurons in the prefrontal cortex control affective state discrimination in mice. *Nat. Neurosci.* **23**, 47–60 (2020).
46. J. B. Burt *et al*., Hierarchy of transcriptomic specialization across human cortex captured by structural neuroimaging topography. *Nat. Neurosci.* **21**, 1251–1259 (2018).
47. F. M. Krienen *et al*., Innovations in primate interneuron repertoire. bioRxiv:10.1101/709501 (23 July 2019).
48. M. J. Grothe *et al*.; Alzheimer's Disease Neuroimaging Initiative, Molecular properties underlying regional vulnerability to Alzheimer's disease pathology. *Brain* **141**, 2755–2771 (2018).
49. S. E. Morgan *et al*., Cortical patterning of abnormal morphometric similarity in psychosis is associated with brain expression of schizophrenia-related genes. *Proc. Natl. Acad. Sci. U.S.A.* **116**, 9604–9609 (2019).
50. I. A. C. Romme, M. A. de Reus, R. A. Ophoff, R. S. Kahn, M. P. van den Heuvel, Connectome disconnectivity and cortical gene expression in patients with schizophrenia. *Biol. Psychiatry* **81**, 495–502 (2017).
51. R. Romero-Garcia *et al*., Schizotypy-related magnetization of cortex in healthy adolescence is colocated with expression of schizophrenia-related genes. *Biol. Psychiatry* **88**, 248–259 (2019).
52. B. B. Lake *et al*., Integrative single-cell analysis of transcriptional and epigenetic states in the human adult brain. *Nat. Biotechnol.* **36**, 70–80 (2018).
53. G. Korotkevich, V. Sukhov, A. Sergushichev, Fast gene set enrichment analysis. bioRxiv:10.1101/060012 (22 October 2019).
54. A. M. Newman *et al*., Determining cell type abundance and expression from bulk tissues with digital cytometry. *Nat. Biotechnol.* **37**, 773–782 (2019).
55. C. A. de Leeuw, J. M. Mooij, T. Heskes, D. Posthuma, MAGMA: Generalized gene-set analysis of GWAS data. *PLoS Comput. Biol.* **11**, e1004219 (2015).
56. H. K. Finucane *et al*.; ReproGen Consortium; Schizophrenia Working Group of the Psychiatric Genomics Consortium; RACI Consortium, Partitioning heritability by functional annotation using genome-wide association summary statistics. *Nat. Genet.* **47**, 1228–1235 (2015).
57. R. D. Hodge *et al*., Conserved cell types with divergent features in human versus mouse cortex. *Nature* **573**, 61–68 (2019).
58. M. S. Lener *et al*., Glutamate and gamma-aminobutyric acid systems in the pathophysiology of major depression and antidepressant response to ketamine. *Biol. Psychiatry* **81**, 886–897 (2017).
59. A. N. van den Pol, Neuropeptide transmission in brain circuits. *Neuron* **76**, 98–115 (2012).
60. J. W. Murrough *et al*., Reduced global functional connectivity of the medial prefrontal cortex in major depressive disorder. *Hum. Brain Mapp.* **37**, 3214–3223 (2016).
61. D. H. Schultz *et al*., Global connectivity of the fronto-parietal cognitive control network is related to depression symptoms in the general population. *Netw. Neurosci.* **3**, 107–123 (2018).
62. G. Hasler, G. Northoff, Discovering imaging endophenotypes for major depression. *Mol. Psychiatry* **16**, 604–619 (2011).
63. D. Cotter *et al*., Reduced neuronal size and glial cell density in area 9 of the dorsolateral prefrontal cortex in subjects with major depressive disorder. *Cereb. Cortex* **12**, 386–394 (2002).
64. W.-S. Chung, N. J. Allen, C. Eroglu, Astrocytes control synapse formation, function, and elimination. *Cold Spring Harb. Perspect. Biol.* **7**, a020370 (2015).
65. M. Santello, N. Toni, A. Volterra, Astrocyte function from information processing to cognition and cognitive impairment. *Nat. Neurosci.* **22**, 154–166 (2019).
66. L. Mariotti *et al*., Interneuron-specific signaling evokes distinctive somatostatin-mediated responses in adult cortical astrocytes. *Nat. Commun.* **9**, 82 (2018).
67. M. Matos *et al*., Astrocytes detect and upregulate transmission at inhibitory synapses of somatostatin interneurons onto pyramidal cells. *Nat. Commun.* **9**, 4254 (2018).
68. G. Douillard-Guilloux, D. Lewis, M. L. Seney, E. Sibille, Decrease in somatostatin-positive cell density in the amygdala of females with major depression. *Depress. Anxiety* **34**, 68–78 (2017).
69. M. R. Montminy, L. M. Bilezikjian, Binding of a nuclear protein to the cyclic-AMP response element of the somatostatin gene. *Nature* **328**, 175–178 (1987).
70. H. Oh *et al*., The role of dendritic brain-derived neurotrophic factor transcripts on altered inhibitory circuitry in depression. *Biol. Psychiatry* **85**, 517–526 (2019).
71. S. M. Dombrowski, C. C. Hilgetag, H. Barbas, Quantitative architecture distinguishes prefrontal cortical systems in the rhesus monkey. *Cereb. Cortex* **11**, 975–988 (2001).
72. Y. Kim *et al*., Brain-wide maps reveal stereotyped cell-type-based cortical architecture and subcortical sexual dimorphism. *Cell* **171**, 456–469.e22 (2017).
73. J. W. Vogel *et al*., A molecular gradient along the longitudinal axis of the human hippocampus informs large-scale behavioral systems. bioRxiv:10.1101/587071 (24 March 2019).
74. B. D. Fulcher, J. D. Murray, V. Zerbi, X.-J. Wang, Multimodal gradients across mouse cortex. *Proc. Natl. Acad. Sci. U.S.A.* **116**, 4689–4695 (2019).
75. R. Romero-Garcia, V. Warrier, E. T. Bullmore, S. Baron-Cohen, R. A. I. Bethlehem, Synaptic and transcriptionally downregulated genes are associated with cortical thickness differences in autism. *Mol. Psychiatry* **24**, 1053–1064 (2019).
76. F. M. Krienen, B. T. T. Yeo, T. Ge, R. L. Buckner, C. C. Sherwood, Transcriptional profiles of supragranular-enriched genes associate with corticocortical network architecture in the human brain. *Proc. Natl. Acad. Sci. U.S.A.* **113**, E469–E478 (2016).
77. J. Richiardi *et al*., BRAIN NETWORKS. Correlated gene expression supports synchronous activity in brain networks. *Science* **348**, 1241–1244 (2015).
78. R. K. Walters *et al*.; 23 and Me Research Team, Transancestral GWAS of alcohol dependence reveals common genetic underpinnings with psychiatric disorders. *Nat. Neurosci.* **21**, 1656–1669 (2018).
79. J. J. Miguel-Hidalgo *et al*., Glial and glutamatergic markers in depression, alcoholism, and their comorbidity. *J. Affect. Disord.* **127**, 230–240 (2010).
80. S. M. Smith, T. E. Nichols, Statistical challenges in "big data" human neuroimaging. *Neuron* **97**, 263–268 (2018).
81. E. S. Finn *et al*., Functional connectome fingerprinting: Identifying individuals using patterns of brain connectivity. *Nat. Neurosci.* **18**, 1664–1671 (2015).
82. N. R. Wray, C. Wijmenga, P. F. Sullivan, J. Yang, P. M. Visscher, Common disease is more complex than implied by the core gene omnigenic model. *Cell* **173**, 1573–1580 (2018).
83. J. T. Baker *et al*., Functional connectomics of affective and psychotic pathology. *Proc. Natl. Acad. Sci. U.S.A.* **116**, 9050–9059 (2019).
84. L. Schmaal *et al*., Subcortical brain alterations in major depressive disorder: Findings from the ENIGMA major depressive disorder working group. *Mol. Psychiatry* **21**, 806–812 (2016).
85. T. C. Ho *et al*., Subcortical shape alterations in major depressive disorder: Findings from the ENIGMA major depressive disorder working group. *Hum. Brain Mapp.*, 1–11, 10.1002/hbm.24988 (2020).
86. D. A. Pizzagalli *et al*., Reduced caudate and nucleus accumbens response to rewards in unmedicated individuals with major depressive disorder. *Am. J. Psychiatry* **166**, 702–710 (2009).
87. D. Scheinost *et al*., Multimodal investigation of network level effects using intrinsic functional connectivity, anatomical covariance, and structure-to-function correlations in unmedicated major depressive disorder. *Neuropsychopharmacology* **43**, 1119–1127 (2018).
88. A. M. Golestani, L. L. Wei, J. J. Chen, Quantitative mapping of cerebrovascular reactivity using resting-state BOLD fMRI: Validation in healthy adults. *Neuroimage* **138**, 147–163 (2016).
89. D. D. Garrett, U. Lindenberger, R. D. Hoge, C. J. Gauthier, Age differences in brain signal variability are robust to multiple vascular controls. *Sci. Rep.* **7**, 10149 (2017).
90. J. Bijsterbosch *et al*., Investigations into within- and between-subject resting-state amplitude variations. *Neuroimage* **159**, 57–69 (2017).
91. D. J. Smith *et al*., Prevalence and characteristics of probable major depression and bipolar disorder within UK biobank: Cross-sectional study of 172,751 participants. *PLoS One* **8**, e75362 (2013).
92. P. T. Costa, R. R. McCrae, "The revised NEO personality inventory (NEO-PI-R)" in *Personality Measurement and Testing* , G. J. Boyle, G. Matthews, D. H. Saklofske, Eds. (The Sage Handbook of Personality Theory and Assessment, Sage, 2008), Vol. 2, pp. 179–198.
93. C. S. Carver, T. L. White, Behavioral inhibition, behavioral activation, and affective responses to impending reward and punishment: The BIS/BAS Scales. *J. Pers. Soc. Psychol.* **67**, 319–333 (1994).
94. D. McNair, M. Lorr, L. Droppleman, *Manual: Profile of Mood States*, (Educational and Industrial Testing Service., San Diego, CA, 1971).
95. C. D. Spielberger, Review of profile of mood states. *Prof. Psychol.* **3**, 387–388 (1972).
96. C. R. Cloninger, A systematic method for clinical description and classification of personality variants. A proposal. *Arch. Gen. Psychiatry* **44**, 573–588 (1987).
97. M. P. Lichy *et al*., Magnetic resonance imaging of the body trunk using a single-slab, 3-dimensional, T2-weighted turbo-spin-echo sequence with high sampling efficiency (SPACE) for high spatial resolution imaging: Initial clinical experiences. *Invest. Radiol.* **40**, 754–760 (2005).
98. R. Romero-Garcia *et al*.; NSPN Consortium, Structural covariance networks are coupled to expression of genes enriched in supragranular layers of the human cortex. *Neuroimage* **171**, 256–267 (2018).
99. D. S. Marcus *et al*., Informatics and data mining tools and strategies for the human connectome project. *Front. Neuroinform.* **5**, 4 (2011).
100. R. S. Desikan *et al*., An automated labeling system for subdividing the human cerebral cortex on MRI scans into gyral based regions of interest. *Neuroimage* **31**, 968–980 (2006).
101. T. Stuart, R. Satija, Integrative single-cell analysis. *Nat. Rev. Genet.* **20**, 257–272 (2019).
102. A. Subramanian *et al*., Gene set enrichment analysis: A knowledge-based approach for interpreting genome-wide expression profiles. *Proc. Natl. Acad. Sci. U.S.A.* **102**, 15545–15550 (2005).
103. H. K. Finucane *et al*.; Brainstorm Consortium, Heritability enrichment of specifically expressed genes identifies disease-relevant tissues and cell types. *Nat. Genet.* **50**, 621–629 (2018).
104. N. G. Skene *et al*.; Major Depressive Disorder Working Group of the Psychiatric Genomics Consortium, Genetic identification of brain cell types underlying schizophrenia. *Nat. Genet.* **50**, 825–833 (2018).
105. K. Watanabe, M. Umićević Mirkov, C. A. de Leeuw, M. P. van den Heuvel, D. Posthuma, Genetic mapping of cell type specificity for complex traits. *Nat. Commun.* **10**, 3222 (2019).
106. J. Chen, E. E. Bardes, B. J. Aronow, A. G. Jegga, ToppGene Suite for gene list enrichment analysis and candidate gene prioritization. *Nucleic Acids Res.* **37**, W305–W311 (2009).